2018 NOAA/AOML/HRD Hurricane Field Program - IFEX

MATURE STAGE EXPERIMENT
Science Description

Investigator(s): Paul Reasor, Jason Dunion (Co-PIs), Sim Aberson, Hui Christophersen, Paul Chang, Joe Cione, John Gamache, Heather Holbach, Ghassan Alaka, Kelly Ryan, Paul Leighton, Robert Rogers, Zorana Jelenak, Jun Zhang (Co-Is)

Requirements: Categories 2–5

Science Objectives:

1) Collect observations targeted at better understanding internal processes contributing to mature hurricane structure and intensity change. These processes include mixing between the eye and eyewall, secondary eyewall formation, the TC diurnal cycle, and gravity waves that emanate from the TC inner core [*IFEX Goal 3*]

2) Collect observations targeted at better understanding the response of mature hurricanes to their changing environment, including changes in vertical wind shear and underlying oceanic conditions [*IFEX Goal 3*]

3) Test new (or improved) technologies with the potential to fill gaps, both spatially and temporally, in the existing suite of airborne measurements in mature hurricanes. These measurements include improved three-dimensional representation of the hurricane wind field, more spatially dense thermodynamic sampling of the boundary layer, and more accurate measurements of ocean surface winds [*IFEX Goal 2*]

Description of Science Objectives:

SCIENCE OBJECTIVE #1: *Collect observations targeted at better understanding internal processes contributing to mature hurricane structure and intensity change. These processes include mixing between the eye and eyewall, secondary eyewall formation, the TC diurnal cycle, and gravity waves that emanate from the TC inner core*
[Internal Processes]

TC DIURNAL CYCLE

Motivation (TC Diurnal Cycle): Numerous studies have documented the existence of diurnal maxima and minima associated with tropical convection. However, predicting the timing and extent of this variability remains a difficult challenge. Recent research using GOES satellite imagery has identified a robust TC diurnal cycle (TCDC) signal in mature storms that includes regularly occurring TC diurnal pulses. TC diurnal pulses can be tracked using new GOES infrared satellite image differencing that reveals a “cool ring” (i.e., diurnal pulse) in the infrared that begins forming near the storm’s inner core around local sunset each day. The TC diurnal pulse continues to propagate away from the storm overnight, reaching areas several hundred km from the storm center by the following afternoon. There appear to be significant structural changes to TCs (as indicated by GOES infrared and microwave (37 and 85 GHz) satellite imagery and P-3 LF radar data)

as TC diurnal pulses move out from the inner core each day and the timing of their radial propagation is remarkably predictable. Although the relationships between the TCDC and TC structure and intensity are unclear at this time, this phenomenon may be an important and fundamental TC process.

Background (TC Diurnal Cycle): Although numerous studies have documented the existence of diurnal maxima and minima associated with tropical oceanic convection and the TC upper-level cirrus canopy, we lack a thorough understanding of the nature and causes of these variations and especially the extent to which these variations are important for TCs. It is well known that the coherent diurnal cycle of deep cumulus convection and associated rainfall is different over the land and ocean (Gray and Jacobson 1977; Yang and Slingo 2001). While over the land it tends to peak in the late afternoon/early evening due to daytime boundary layer heating, over the ocean it peaks in the early morning. In addition, Gray and Jacobson (1977), Mapes and Houze (1993), and Liu and Moncrieff (1998) found that the oceanic peak was more prominent when the preexisting convection was more intense and associated with an organized weather system such as an African easterly wave or mesoscale convective system. Numerous studies have also highlighted diurnal changes in the cirrus anvils of tropical deep convection and TCs. Weikmann et al. (1977) noted that anvils emanating from large cumulonimbus clouds tended to grow preferably between 2200 and 0300 local standard time (LST). Browner et al. (1977) found that the areal extent of the TC cirrus canopy was a minimum at 0300 LST and a maximum at 1700 LST and suggested that this diurnal oscillation might be important for the TC. More recently, Kossin (2002) used storm-centered GOES infrared imagery to calculate azimuthally averaged brightness temperatures and create Hovmöller-type diagrams of brightness temperature diurnal oscillations over time. That study concluded that although a clear diurnal oscillation of the TC cirrus canopy was present at larger radii (e.g., 300 km), few storms exhibited diurnal oscillation signals in their innermost 100 km. It was hypothesized that different processes might be forcing periodic oscillations in the TC deep inner-core convection and the TC cirrus canopy.

Dunion et al. (2014) examined all North Atlantic major hurricanes from 2001 to 2010 and documented a phenomenon they referred to as the TC diurnal cycle and associated diurnal pulses in mature TCs. They found an intriguing diurnal pulsing pattern that appears to occur with remarkable regularity through a relatively deep layer of the TC. Storm-centered GOES and Meteosat infrared imagery were used to create 6-h brightness temperature difference fields of the storm's inner core and its surrounding environment (Radius, R, 5 100–600 km). The imagery reveals periodic oscillations of cooling and warming in the IR brightness temperature field over time. One prominent characteristic of these oscillations is a cold ring (i.e., local cooling of the brightness temperatures with time) that begins forming in the storm's inner core (R~≤150 km; Rogers et al. 2012) near the time of sunset each day. This cold ring feature (that they referred to as a TC diurnal pulse) continues to move away from the storm overnight, reaching areas several hundred kilometers from the circulation center by the following afternoon and is well-predicted by a TC diurnal clock that they developed (Fig. MA-1). A marked warming of the cloud tops

occurs behind this propagating feature and structural changes in the storm are noted as it moves away from the inner core. This systematic variation of cloud-top temperatures suggests that TC diurnal pulses are a distinguishing characteristic of the TCDC and may have implications for TC intensity change and structure.

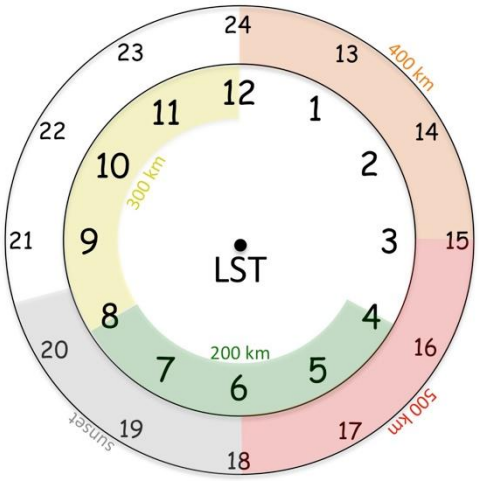

Figure MA-1. *Conceptual 24-hr TCDC clock that estimates the radial location of TC diurnal pulses propagating away from storm. TC diurnal pulses typically form around local sunset (~1800–2030 LST, gray shading) and begin to propagate away from the inner core, passing 200 km radius at ~0400–0800 LST (green shading) the following morning. They reach 400 km radius at ~1200–1500 LST (orange shading) in the early to middle afternoon.*

Hypotheses (TC Diurnal Cycle): The TC diurnal cycle and associated TC diurnal pulses manifest as semi-circular rings of enhanced convection that radially propagate away from the storm each day and are associated with periods of enhanced upper-level outflow and lower-level inflow that extend through a relatively deep layer of the troposphere.

Aircraft Pattern/Module Descriptions:

P-3 Pattern #1: Internal Processes (TC Diurnal Cycle)

For TCs exhibiting TC diurnal cycle signals, perform any standard pattern that provides symmetric coverage (e.g. Rotated Figure-4, Figure-4, Butterfly).

G-IV Pattern #1: Internal Processes (TC Diurnal Cycle)

For TCs exhibiting TC diurnal cycle signals, perform a standard G-IV Star with circumnavigation (optimal) or star (minimal) pattern.

Analysis Strategy (TC Diurnal Cycle): This objective seeks to observe the formation and evolution of the TC diurnal cycle and associated TC diurnal pulses. GPS dropsonde and radar observations will be used to analyze both the inner-core and environmental kinematics and thermodynamics that may lead to the formation of TC diurnal pulses and to document the kinematics, thermodynamics, and precipitation patterns that are associated with radially propagating TC diurnal pulses at various stages of their evolution.

References (TC Diurnal Cycle):

Browner, S. P., W. L. Woodley, and C. G. Griffith, 1977: Diurnal oscillation of cloudiness associated with tropical storms. *Mon. Wea. Rev*., **105**, 856–864.

Dunion, J.P., C.D. Thorncroft, and C.S. Velden, 2014: The tropical cyclone diurnal cycle of mature hurricanes. *Mon. Wea. Rev.,* **142***,* 3900–3919.

Gray, W. M., and R. W. Jacobson, 1977: Diurnal variation of deep cumulus convection. *Mon. Wea. Rev*., **105**, 1171–1188.

Kossin, J. P., 2002: Daily hurricane variability inferred from GOES infrared imagery. *Mon. Wea. Rev*., **130**, 2260–2270.

Liu, C., and M. W. Moncrieff, 1998: A numerical study of the diurnal cycle of tropical oceanic convection. *J. Atmos. Sci*., **55**, 2329–2344.

Mapes, B. E., and R. A. Houze Jr., 1993: Cloud clusters and superclusters over the oceanic warm pool. *Mon. Wea. Rev*., **121**, 1398–1415.

Rogers, R. F., S. Lorsolo, P. Reasor, J. Gamache, and F. Marks, 2012: Multiscale analysis of tropical cyclone kinematic structure from airborne Doppler radar composites. *Mon. Wea. Rev*., **140**, 77–99.

Weickmann, H. K., A. B. Long, and L. R. Hoxit, 1977: Some examples of rapidly growing oceanic cumulonimbus clouds. *Mon. Wea. Rev*., **105**, 469–476.

Yang, G., and J. Slingo, 2001: The diurnal cycle in the tropics. *Mon. Wea. Rev*., **129**, 784–801.

GRAVITY WAVE

Motivation (Gravity Wave): Internal gravity waves are ubiquitous in the atmosphere and are continuously generated by deep moist convection around the globe. Gravity waves play a critical role in the dynamical adjustment processes that keep the atmosphere close to hydrostatic and geostrophic wind balance, by redistributing localized heating over larger distances. Numerical simulations showed gravity waves radiating from the eyewall region to the outer core in TCs. TC convection produces gravity waves that propagate both upward and outward. This module is designed to observe smaller scale gravity waves, with radial wavelengths of 2 to 20 km, that radiate outward from the TC core with phase speeds of 20 to 30 m s^{-1}. The goal is to quantify how the characteristics of these waves are tied to TC intensity and intensity change.

Background (Gravity Wave): Gravity waves exist due to the natural restoring force associated with the static stability of the atmosphere (Markowski and Richardson 2010; Sutherland 2010). Most gravity wave generation is associated with three processes: 1) the interaction of the atmospheric flow with topography, 2) rapidly evolving imbalances of the large-scale flow, and 3) disruptions to the atmosphere by moist convection. Visual evidence for these waves existing in TCs was documented in the early study by Black (1983), who analyzed features in cloud tops using stereoscopic analysis of photographs taken from hand-held cameras on the Skylab space station. Simulations with mesoscale atmospheric models have reproduced these features, which generally have wavelengths of tens to hundreds of km (Kim et al. 2009). These waves propagate long distances and their influences on the atmospheric boundary layer have also been observed (Niranjan-Kumar et al. 2014).

These waves can be observed by research aircraft and surface instruments (Nolan and Zhang 2017). The flight-level data reveal waves with radial wavelengths of 2–10 km, and by compositing the data from inbound and outbound flight legs separately, an outward phase speed of 20–25 m s^{-1} can be inferred. Data from a research buoy in the Pacific also show evidence for the effects of the gravity waves on surface pressure and wind speed, with periods around 1000 s and 2000 s. Numerical simulations reproduce these waves and indicate distinct vertical structures for the dominant modes, with peaks in amplitude of vertical velocity near the tropopause and in the lower troposphere (Nolan and Zhang 2017). The simulations also indicate that TC intensity can be correlated with the amplitudes of these wave signals. Thus, analysis of atmospheric gravity waves may be a more direct approach for remote monitoring of TC intensity.

Hypotheses (Gravity Wave): Gravity waves radiating from the TCs inner core are prevalent in TCs and their wave amplitudes correlate with TC intensity.

Aircraft Pattern/Module Descriptions:

P-3 Module #1: Internal Processes (Gravity Wave)

For mature stage TCs, after completing Figure-4 pattern, at the end of the last leg, continue outward to distance of 160 n mi from the center, or further, if possible. Then turn P-3 back to the eye. This module ideally should be conducted in quadrant with the least rainband activity, typically the upshear right or right-real quadrant.

Analysis Strategy (Gravity Wave): This module seeks to observe the characteristics of the TC gravity waves. Flight-level wind observations will be used to analyze the wavelengths and amplitudes of these waves. The vertical velocity will be quality controlled by correcting the attack angle and dynamical pressure using specially designed modules conducted by calibration flights before each hurricane season (Zhang 2010; Zhang and Drennan 2012). To avoid the contamination of the spectra by convection near the eyewall, only data from at least 100 km away from the storm center are used. The power spectrum will be computed using a fast Fourier Transform (FFT) algorithm to estimate the peak wavelengths of these waves.

References (Gravity Wave):

Black, P. G., (1983), Tropical storm structure revealed by stereoscopic photographs from Skylab. *Adv. Space Res.*, **2**, No. 6, 115–124.

Kim, S.-Y., H.-Y. Chun, and D. L. Wu (2009), A study on stratospheric gravity waves generated by Typhoon Ewiniar: Numerical simulations and satellite observations. *J. Geophys. Res*., **114**, D22104.

Markowski, P., and Y. Richardson (2010), *Mesoscale meteorology in mid-latitudes*. Wiley-Blackwell, Hoboken, New Jersey, 430 pp.

Niranjan Kumar, K., Ch. Kanaka Rao, A. Sandeep, and T. N. Rao (2014), SODAR observations of inertia-gravity waves in the atmospheric boundary layer during the passage of tropical cyclone. *Atmos. Sci. Lett*., **15**, 120–126.

Nolan, D.S., and J.A. Zhang, 2017: Spiral gravity waves radiating from tropical cyclones. Geophysical Research Letters, 44(8):3924–3931, doi:10.1002/2017GL073572.

Sutherland, B. R., *Internal Gravity Waves* (2010). Cambridge University Press, New York, 377 pp.

Zhang, J. A., (2010), Spectral characteristics of turbulence in the hurricane boundary layer over the ocean between the outer rainbands. *Quart. J. Roy. Meteorol. Soc*., **136**, 918–926.

Zhang, J. A., and W. M. Drennan (2012), An observational study of vertical eddy diffusivity in the hurricane boundary layer. *J. Atmos. Sci.,* **69**, 3223–3236.

SECONDARY EYEWALL FORMATION (SEF)

Motivation (SEF): Secondary eyewall formation (SEF) and eyewall replacement cycles (ERCs) frequently occur during the mature phase of the TC lifecycle. These processes typically result in a halting of the intensification of a TC, and occasionally lead to a temporary weakening as the secondary eyewall becomes the dominant eyewall (Sitkowski et al. 2011). Additionally, they typically lead to a significant broadening of the wind field, increasing the total kinetic energy of the storm and thus the risks from storm surge. Statistical analysis of a 10-year (1997–2007) dataset shows that 77% of major hurricanes (120 knots or higher) in the Atlantic Ocean, 56% in the eastern Pacific, 81% in the western Pacific, and 50% in the Southern Hemisphere underwent at least one ERC (Hawkins and Helveston 2008). Despite the relative frequency of their occurrence, operational forecasting of SEF/ERCs remains a great challenge, partly since there is no consensus on the mechanisms responsible for SEF or ERC.

Background (SEF): There are a wide variety of studies that aim to understand SEF and ERC with different emphases on the internal dynamics and external environmental forcing. The axisymmetric balanced flow, constrained by heat and tangential momentum forcing, generally satisfies gradient wind and hydrostatic balance above the boundary layer (BL) (Abarca and Montgomery 2013). From the perspective of diabatic forcing, Rozoff et al. (2012) proposed that a sustained azimuthal-mean latent heating outside of the primary eyewall could lead to SEF. This hypothesis was supported by the numerical simulations given by Zhu and Zhu (2014). In a similar sense, diabatic heating/cooling associated with rainbands plays an important role in the structure and intensity change of the storm (Wang 2009; Li et al. 2014; Moon and Nolan 2010; Didlake and Houze 2013a, b) and thus they may also contribute to the SEF/ERC. Didlake and Houze (2013a) proposed that there exists a critical zone where sufficiently high vertical shear of the radial wind can limit the altitude of the convectively induced supergradient flow, leading to low-level convergence in this radial zone and allowing the convection to develop into a secondary eyewall. Corbosiero and Torn (2016) proposed a hypothesis that an increase of convergence induced by the cold pool that formed from convectively-driven downdrafts and low-level radial inflow could enhance rainband convection and lead to SEF. The roles of convective and stratiform heating profiles in rainbands in modifying hurricane structure and intensity, and potentially SEF, is an area of ongoing research.

Montgomery and Kallenbach (1997) proposed that vortex Rossby wave (VRW) interaction with the mean flow may contribute to SEF. VRWs, supported by the radial vorticity gradient outside of the radius of the maximum wind (RMW), propagate from the primary eyewall radially outward until they reach their stagnation radius. At this stagnation radius, inward-moving cyclonic eddy momentum may contribute to SEF. The role of VRWs in SEF is further examined in high-resolution hurricane simulations by Abarca and Corbosiero (2011). Judt and Chen (2010), by contrast, downplayed the importance of VRWs, and instead attributed the large accumulation of convectively generated PV through eddy heating in the rainband region as an essential factor for SEF.

In contrast to the balanced arguments discussed above, unbalanced dynamics in the BL have also been recognized as an important element in SEF. In this framework, the axisymmetric flow in the BL does not satisfy gradient wind and thermal wind balance. Several studies (Wu et al. 2011; Huang et al. 2012; Abarca and Montgomery 2013) have pointed out that the precursors of SEF include the broadening of the tangential wind field and the intensification of inflow in the BL, followed by development of supergradient winds and an enhanced horizontal convergence. In-situ observations also demonstrated this existence of supergradient flow (Didlake and Houze 2011; Bell et al. 2012). Kepert (2013) specifically examined the role of the BL in a balanced vortex framework. He proposed that the BL contributed to the SEF and ERC through a positive feedback mechanism that involves a local enhancement of the radial gradient of vorticity, frictionally forced updraft and convection. Moon et al. (2010) attributed the local vorticity enhancement from processes such as rainband convection.

To test the varying mechanisms proposed to explain SEF and ERC, it is important to obtain kinematic and thermodynamic observations near the eyewall and rainbands. In particular, since most previous analyses focus on azimuthally averaged quantities, it is important to obtain adequate azimuthal and radial sampling both near the primary eyewall and a potentially-developing secondary eyewall. For example, Abarca et al. (2016) pointed out the lack of data particularly at radial distance between 120–200 km in Hurricane Edouard (2014). Additionally, some measure of kinematic and thermodynamic structures along a rainband/developing secondary eyewall can be used to evaluate the along-band structures (Wang 2009; Moon and Nolan 2010; Didlake and Houze 2011, 2013a,b). Observations sampled through this module can be used to evaluate the different proposed mechanisms of SEF and ERC. Data-impact studies on TC analyses and forecasts can also be conducted using the OSSE approach to find optimal sampling strategies for the prediction of SEF/ERC. If this module is flown every 12 h (e.g., in conjunction with the TDR experiment), then the temporal resolution will provide an opportunity to evaluate the importance of the various proposed mechanisms at different stages in the evolution of the secondary eyewall. The dataset from this module eventually will benefit our understanding of the dynamic and physical processes that are responsible for SEF/ERC.

The main objectives of the SEF/ERC module are:

- Perform analyses with sampled observations to examine key factors that are responsible for SEF/ERCs;
- Validate key features linked with different hypotheses of SEF/ERCs using observations;
- Conduct OSE/OSSE studies to optimize sampling strategies for improving SEF/ERC predictions;
- Improve understanding of the dynamic and physical processes of SEF/ERCs.

Hypotheses (SEF): Secondary eyewall formation could be attributed from an unbalanced boundary layer spin-up paradigm. The precursors of SEF include the broadening of the

tangential wind field and the intensification of inflow in the boundary layer, followed by development of supergradient winds and an enhanced horizontal convergence.

Aircraft Pattern/Module Descriptions:

P-3 Module #2: Internal Processes (Pre-SEF)
P-3 Module #3: Internal Processes (Post-SEF)
G-IV Module #1: Internal Processes (SEF)

> This module focuses on mature hurricanes (e.g., category 2 or stronger) with a well-defined eye as seen in visible, infrared, and microwave satellite imagery. Sampling can be achieved in combination with the P-3 Doppler Wind Lidar, Coyote UAS, P-3 and G-IV dropsondes. This module can generally be flown in conjunction with TDR Experiment survey patterns, with the addition of either a spiral pattern (Pre-SEF) or moat circumnavigation (Post-SEF) added onto the survey. The module can also be flown for the TC Diurnal Cycle objective.

Analysis Strategy (SEF): Data collected by the pre-SEF module can be used to diagnose different roles in SEF. Specifically, gradient wind (and departures thereof) within and above the BL can be calculated from dropsondes; tangential winds and vorticity can be calculated from dropsonde, Doppler radar, flight-level, and DWL measurements; and moist static energy calculation, can be calculated from dropsondes. Observations that are collected can also be used to conduct data impact studies as well as provide insights for OSSE studies. Data measured by the post-SEF module would be useful to diagnose the formation and characteristics of the moat region and its role in ERC. Azimuthal coverage of the data would be particularly important to carry out analysis to validate different hypotheses of SEF/ERC.

References (SEF):

Abarca, S. F., and K. L. Corbosiero, 2011: Secondary eyewall formation in WRF simulations of Hurricanes Rita and Katrina (2005). *Geophys. Res. Lett.*, **38**, 1–5.

Abarca, S. F., and M. T. Montgomery, 2013: Essential Dynamics of Secondary Eyewall Formation. *J. Atmos. Sci.*, **70**, 3216–3230.

Abarca, S. F., M. T. Montgomery, S. Braun, and J. Dunion, 2016: Secondary Eyewall Dynamics as Captured by an Unprecedented Array of GPS Dropsondes Deployed into Edouard 2014, 32nd Conf. on Hurricanes and Tropical Meteorology, San Juan, PR.

Bell, M. M., M. T. Montgomery, and W.-C. Lee, 2012: An Axisymmetric View of Concentric Eyewall Evolution in Hurricane Rita (2005). *J. Atmos. Sci.*, **69**, 2414–2432.

Corbosiero K. L., and R. D. Torn, 2016: Diagnosis of Secondary Eyewall Formation Mechanisms in Hurricane Igor (2010), 32nd Conf. on Hurricanes and Tropical Meteorology, San Juan, PR.

Didlake Jr., A. C., and R. A. Houze, 2011: Kinematics of the Secondary Eyewall Observed in Hurricane Rita (2005). *J. Atmos. Sci.*, **68**, 1620–1636.

Didlake, Jr., A. C., and R. A. Houze, 2013a: Convective-Scale Variations in the Inner-Core Rainbands of a Tropical Cyclone. *J. Atmos. Sci.,* 70, 504–523.

Didlake, A. C., and R. A. Houze, 2013b: Dynamics of the Stratiform Sector of a Tropical Cyclone Rainband. *J. Atmos. Sci.*, 70, 1891–1911.

Hawkins, J. D., and M. Helveston, 2008: Tropical cyclone multiple eyewall characteristics. Preprints, 28th Conf. on Hurricanes and Tropical Meteorology, Amer. Meteor. Soc., Orlando, FL.

Huang, Y.-H., M. T. Montgomery, and C.-C. Wu, 2012: Concentric Eyewall Formation in Typhoon Sinlaku (2008). Part II: Axisymmetric Dynamical Processes. *J. Atmos. Sci.*, 69, 662–674.

Judt, F., and S. S. Chen, 2010: Convectively Generated Potential Vorticity in Rainbands and Formation of the Secondary Eyewall in Hurricane Rita of 2005. *J. Atmos. Sci.*, 67, 3581–3599.

Kepert, J. D., 2013: How does the boundary layer contribute to eyewall replacement cycles in axisymmetric tropical cyclones? *J. Atmos. Sci.*, 70, 2808–2830.

Li, Q., Y. Wang, and Y. Duan, 2014: Effects of Diabatic Heating and Cooling in the Rapid Filamentation Zone on Structure and Intensity of a Simulated Tropical Cyclone. *J. Atmos. Sci.,* 71, 3144–3163.

Montgomery, M. T., and R. J. Kallenbach, 1997: A theory for vortex Rossby-waves and its application to spiral bands and intensity changes in hurricanes. *Quart. J. Roy. Meteor. Soc.,* 123, 435–465.

Moon, Y., and D. S. Nolan, 2010: The Dynamic Response of the Hurricane Wind Field to Spiral Rainband Heating. *J. Atmos. Sci.*, 67, 1779–1805.

Moon, Y., D. S. Nolan, and M. Iskandarani, 2010: On the Use of Two-Dimensional Incompressible Flow to Study Secondary Eyewall Formation in Tropical Cyclones. *J. Atmos. Sci.*, **67**, 3765–3773.

Rozoff, C. M., D. S. Nolan, J. P. Kossin, F. Zhang, and J. Fang, 2012: The Roles of an Expanding Wind Field and Inertial Stability in Tropical Cyclone Secondary Eyewall Formation. *J. Atmos. Sci.,* 69, 2621–2643.

Sitkowski, M., J. P. Kossin, and C. M. Rozoff, 2011: Intensity and Structure Changes during Hurricane Eyewall Replacement Cycles. *Mon. Wea. Rev.,* 139, 3829–3847.

Wang, Y., 2009: How Do Outer Spiral Rainbands Affect Tropical Cyclone Structure and Intensity?. *J. Atmos. Sci.*, 66, 1250–1273.

Wu, C.-C., Y.-H. Huang, and G.-Y. Lien, 2012: Concentric Eyewall Formation in Typhoon Sinlaku (2008). Part I: Assimilation of T-PARC Data Based on the Ensemble Kalman Filter (EnKF). *Mon. Wea. Rev.*, 140, 506–527.

Zhu, Z.-D., and P. Zhu, 2014: The role of outer rainband convection in governing the eyewall replacement cycle in numerical simulations of tropical cyclones*, J. Geophys. Res. Atmos*., 119, 8049–8072.

EYE-EYEWALL MIXING

Motivation and Background (Eye-Eyewall Mixing): Eyewall mesovortices have been hypothesized to mix high-entropy air from the eye into the eyewall, thus increasing the amount of energy available to the hurricane. Signatures of such mesovortices have been seen in cloud formations within the eyes of strong TCs, in radar reflectivity signatures (Hurricane Fabian), and from above during aircraft penetrations (Hurricanes Hugo and Felix). Doppler radar was able to sample such features in Hurricanes Hugo and Felix, though interpretation with sparse observations through the small features has been difficult. Dropwindsondes released in very intense tropical cyclones, in conjunction with large-eddy simulations, have provided some thermodynamic data. However, the kinematic and thermodynamic structures of these features have never been directly observed. Observations within the eye near or below the inversion can allow for the study of the these mesovortices and improve knowledge of small-scale features and intensity changes in very strong TCs.

Hypotheses (Eye-Eyewall Mixing): Eyewall mesovortices play an important role in TC intensity change.

Aircraft Pattern/Module Descriptions:

P-3 Module #4: Internal Processes (Eye-Eyewall Mixing)

This is a break-away pattern that is compatible with any standard pattern with an eye passage (all P-3 patterns except the Square spiral or Lawnmower). The P-3 will penetrate the eyewall at the standard-pattern altitude. Once inside the eye, the

P-3 will descend to a safe altitude below the inversion while performing a Figure-4 pattern. The leg lengths will be determined by the eye diameter, with the ends of the legs at least 2 n mi from the edge of the eyewall. Upon completion of the descent, the P-3 will circumnavigate the eye about 2 n mi from the edge of the eyewall in the shape of a pentagon or hexagon. Time permitting; another Figure-4 will be performed during ascent to the original flight level. Depending upon the size of the eye, this pattern should take between 0.5 and 1 h. The module need only be done once and will then be evaluated for the future.

Analysis Strategy (Eye-Eyewall Mixing): The data will be examined to look for meso- or miso-scale vortices at the eye-eyewall interface. Analyses with an advanced data assimilation system will also be conducted.

References (Eye-Eyewall Mixing):

Aberson, S. D., J. A. Zhang, and K. Nunez-Ocasio, 2017: An extreme event in the eyewall of Hurricane Felix on 2 September 2007. *Mon. Wea. Rev.,* in press.

Aberson, S. D., J. P. Dunion, and F. D. Marks, 2006: A photograph of a wavenumber-2 asymmetry in the eye of Hurricane Erin. *J. Atmos. Sci.*,**63**, 387–391.

Aberson, S. D., M. T. Montgomery, M. M. Bell, and M. L. Black. 2006: Hurricane Isabel (2003): New insights into the physics of intense storms. Part II: Extreme localized wind. *Bull. Amer. Met. Soc.,* **87**, 1349–1354.

Marks, F.D., P.G. Black, M.T. Montgomery, and R.W. Burpee. Structure of the eye and eyewall of Hurricane Hugo (1989). *Mon. Wea. Rev.,* **136**, 1237–1259.

Rogers, R. F., S. Aberson, M. M. Bell, D. J. Cecil, J. D. Doyle, T. B. Kimberlain, J. Morgerman, L. K. Shay, and C. Velden, 2017: Re-writing the tropical record books: The extraordinary intensification of Hurricane Patricia (2015). *Bull. Amer. Met. Soc.,* in press.

Stern, D. P., G. H. Bryan, and S. D. Aberson, 2016: Extreme low-level updrafts and wind speeds measured by dropsondes in tropical cyclones.*Mon. Wea. Rev.,* **144**, 2177–2204.

MATURE STAGE EXPERIMENT
Science Description

SCIENCE OBJECTIVE #2: *Collect observations targeted at better understanding the response of mature hurricanes to their changing environment, including changes in vertical wind shear and underlying oceanic conditions* [Environment Interaction]

TC IN SHEAR

Motivation (TC in Shear): Although most TCs in HRD's data archive experience some degree of vertical wind shear (VWS), the timing of flights with respect to the shear evolution and the spatial sampling of kinematic and thermodynamic variables have not always been carried out in an optimal way for testing hypotheses regarding shear-induced modifications of TC structure and their impact on intensity change (see below). This objective will sample the TC at distinct phases of its interaction with VWS and measure kinematic and thermodynamic fields with the azimuthal and radial coverage necessary to test existing hypotheses.

Background (TC in Shear): Recently, Riemer et al. (2010) and Riemer et al. (2013) have proposed an intensity modification mechanism rooted in a balance-dynamics framework. They argue that balanced vorticity asymmetry at low levels, generated outside the core through shear forcing, organizes convection outside the eyewall into a wavenumber-1 pattern through frictional convergence. Downdrafts associated with this vortex-scale convective asymmetry arise as precipitation generated by the convective updrafts falls into unsaturated air below. In their simulations, the downdrafts led to a vortex-scale transport of low equivalent potential temperature (θ_e) air into the inflow layer and disruption of the TC heat engine (Emanuel 1986, 1991). If particularly low θ_e air at lower to middle levels of the environment is able to reach the core region where convective enhancement occurs, the thermodynamic impacts of the downward transport of low θ_e air would be enhanced. Riemer and Montgomery (2011) proposed a simple kinematic model for this environmental interaction, quantifying the shear-induced distortion of the "moist envelope" surrounding the TC core as a function of shear strength, vortex size, and vortex intensity.

In the simulations of Riemer et al. (2010), the TC core region developed vertical tilt following its initial encounter with VWS, but then realigned, i.e., the vortex was resilient. The problem of dynamic resilience focuses on the ability of the TC to maintain a vertically-coherent vortex structure as it experiences vertical shearing. Jones (1995) found that coupling between vertical layers, and the tendency for the upper- and lower-level potential vorticity (PV) of the cyclonic core to precess upshear, restricts the development of vertical tilt that would otherwise occur through differential advection. For small-amplitude tilt, Reasor et al. (2004) developed a balance theory for the shear forcing of vortex tilt in which the tilt asymmetry behaves as a vortex-Rossby wave. In this vortex-Rossby wave framework, they developed a heuristic model for the TC in shear, which predicts a left-of-shear tilt equilibrium. Furthermore, they demonstrated that the evolution towards this equilibrium tilt state depends not only on intrinsic scales of the flow (e.g., Rossby number and Rossby deformation radius), but also on the radial

distribution of (potential) vorticity in the core region. Reasor and Montgomery (2015) have recently evaluated this heuristic model. The model is capable of predicting the enhancement of resilience that arises as the PV gradient outside the core increases. Even when moist neutral conditions exist within the eyewall, the model still describes the long-time evolution of the tilt asymmetry outside the eyewall.

Hypotheses (TC in Shear): Vertical wind shear inhibits TC intensification through the downward transport of low-entropy air into the inflow layer outside the eyewall, brought on by vortex-tilt-induced organization of convection there.

Aircraft Pattern/Module Descriptions:

P-3 Pattern #1: Environment Interaction (TC in Shear)

Prior to an increase in vertical wind shear, perform a Figure-4 pattern (orientation chosen for efficiency) with TDR to obtain the TC core structure. As time permits, the aircraft executes a second, rotated Figure-4 pattern.

P-3 Pattern #2: Environment Interaction (TC in Shear)

Following an increase in vertical wind shear (~12 h after *P-3 Pattern #1: Environment*), perform a single Figure-4 pattern with TDR to obtain the TC core-region structure. Then travel downwind to set up a rotated Figure-4 pattern with truncated radial legs. The radial legs should extend just outside the primary mesoscale region of convection radially beyond (~15–30 n mi) the eyewall. Dropsondes should be launched within and downwind of the convective region outside the eyewall in such a way as to sample low-entropy air spiraling into the eyewall within the boundary layer. Repeat every 12 h.

G-IV Pattern #1: Environment Interaction (TC in Shear)

Perform storm-relative environmental TDR and dropsonde sampling through clockwise circumnavigation, starting at 150 n mi, moving inward to 90 n mi, and finishing at 60 n mi. This pattern should be coordinated with *P-3 Pattern #1: Environment Interaction (TC in Shear)* during the pre-shear stage and then 24 h later with *P-3 Pattern #2: Environment Interaction (TC in Shear)*. A primary objective of the coordinated P-3 and G-IV dropsonde sampling is to document the evolution of the moist envelope surrounding the core.

Analysis Strategy (TC in Shear): The basic analysis follows that presented in recent observational studies of the vertically sheared TC (Reasor et al. 2009; Reasor and Eastin 2012; Reasor et al. 2013; Rogers et al. 2013; Zhang et al. 2013). The analysis includes: low-wavenumber kinematic structure of the core region above the boundary layer, vortex tilt, and local VWS derived from airborne Doppler radar observations; low-wavenumber kinematic structure of the boundary layer derived from SFMR and dropsonde

measurements; low-wavenumber thermodynamic structure within and above the boundary layer derived from dropsondes and flight-level measurements; and convective burst statistics derived from Doppler radar observations. New elements of the analysis will include: 3-D kinematic structure out to at least 4–5xRMW using radar observations; low-wavenumber kinematic, thermodynamic, and moisture structures out to 150 n mi using G-IV radar and dropsonde observations; high azimuthal and radial representation of the inflow structure downwind of the mesoscale-organized convection radially outside the eyewall.

References (TC in Shear):

Emanuel, K. A., 1986: An air-sea interaction theory for tropical cyclones. Part I: Steady-state maintenance. *J. Atmos. Sci.*, **43**, 585–605.

Emanuel, K. A., 1991: The theory of hurricanes. *Annu. Rev. Fluid Mech.*, **23**, 179–196.

Jones, S. C., 1995: The evolution of vortices in vertical shear. I: Initially barotropic vortices. *Quart. J. Roy. Meteor. Soc.*, **121**, 821–851.

Reasor, P. D., M. T. Montgomery, and L. D. Grasso, 2004: A new look at the problem of tropical cyclones in vertical shear flow: Vortex resiliency. *J. Atmos. Sci.*, **61**, 3–22.

Reasor, P. D., M. Eastin, and J. F. Gamache, 2009: Rapidly intensifying Hurricane Guillermo (1997). Part I: Low-wavenumber structure and evolution. *Mon. Wea. Rev.*, **137**, 603–631.

Reasor, P. D., and M. D. Eastin, 2012: Rapidly intensifying Hurricane Guillermo (1997). Part II: Resilience in shear. *Mon. Wea. Rev.*, **140**, 425–444.

Reasor, P. D., R. Rogers, and S. Lorsolo, 2013: Environmental flow impacts on tropical cyclone structure diagnosed from airborne Doppler radar composites. *Mon. Wea. Rev.,***141**, 2949–2969.

Reasor, P. D., and M. T. Montgomery, 2015: Evaluation of a heuristic model for tropical cyclone resilience. *J. Atmos. Sci*., **72**, 1765–1782.

Riemer, M., M. T. Montgomery, and M. E. Nicholls, 2010: A new paradigm for intensity modification of tropical cyclones: thermodynamic impact of vertical wind shear on the inflow layer. *Atmos. Chem. Phys.*, **10**, 3163–3188.

Riemer, M., and M. T. Montgomery, 2011: Simple kinematic models for the environmental interaction of tropical cyclones in vertical wind shear. *Atmos. Chem. Phys.*, **11**, 9395–9414.

Riemer, M., M. T. Montgomery, and M. E. Nicholls, 2013: Further examination of the thermodynamic modification of the inflow layer of tropical cyclones by vertical wind shear. *Atmos. Chem. Phys.*, **13**, 327–346.

Rogers, R., P. Reasor, and S. Lorsolo, 2013: Airborne Doppler observations of the inner-core structural differences between intensifying and steady-state tropical cyclones. *Mon. Wea. Rev.*, **141**, 2970–2971.

Zhang, J. A., R. F. Rogers, P. D. Reasor, E. W. Uhlhorn, and F. D. Marks Jr., 2013: Asymmetric hurricane boundary layer structure in relation to the environmental vertical wind shear from dropsonde composites. *Mon. Wea. Rev.*, **141**, 3968–3984.

ARC CLOUD

Motivation (Arc Cloud): Arc clouds are common features in mid-latitude thunderstorms and mesoscale convective systems. They often denote the presence of a density current that forms when dry mid-level (~600–850 hPa) air has interacted with precipitation. The convectively-driven downdrafts that result reach the surface/near-surface and spread out from the convective core of the thunderstorm. Substantial arc clouds (i.e. >55 n mi (100 km) in length and lasting for several hours) are also common features in the tropics (Fig. MA-2), particularly on the periphery of African easterly waves (AEWs) and TCs. However, the physical processes responsible for such tropical arc clouds as well as their impacts on the short-term evolution of their parent disturbances are not well understood.

Background (Arc Cloud): Large low-level thunderstorm outflow boundaries emanating from TCs have been previously documented and have been hypothesized to occur when high vertical wind shear promotes the intrusion of dry mid-level air toward the TC eyewall (Knaff and Weaver 2000). However, the mid-level moisture found in the *moist tropical* North Atlantic sounding described by Dunion (2011) is hypothesized to be insufficiently dry to generate extensive near-surface density currents around an AEW or TC. However, Dunion (2011) also described two additional air masses that are frequently found in the tropical North Atlantic and Caribbean during the summer months and could effectively initiate the formation of large arc clouds: (1) the Saharan Air Layer (*SAL*) and (2) *mid-latitude dry air intrusions*. Both of these air masses were found to contain substantially dry air (~50% less moisture than the *moist tropical* sounding) in the mid-levels that could support convectively-driven downdrafts and large density currents. Furthermore, outward-propagating arc clouds on the periphery of AEWs or TCs could be enhanced by near-surface super-gradient winds induced by the downward transport of high momentum air. Since most developing tropical disturbances in the North Atlantic are associated with a mid-level jet and/or mesoscale convective vortex near a state of gradient balance, any convectively-driven downdrafts would inject high momentum air into a near-surface environment that often contains a weaker horizontal pressure gradient. In such cases, density currents may be temporarily enhanced during local adjustments to gradient balance. Finally, tropical arc clouds may be further

enhanced by outward-propagating diurnal pulses that originate from the convective core of the tropical disturbance (see the TC Diurnal Cycle objective). New GOES IR TC diurnal cycle imagery indicates that arc clouds tend to form along the leading edge of outwardly propagating diurnal pulses that are associated with the TC diurnal cycle. The diurnal pulses reach peripheral radii where low to mid-level dry air is often located (e.g. Radius, R, 300–500 km) at remarkably predictable times of day (e.g. 400 km at ~1200–1500 LST). Therefore, UW-CIMSS real-time TC diurnal cycle and visible satellite imagery, as well as P-3 LF radar data (where TC diurnal pulses are denoted by 25+ dBZ semi-circular convective bands propagating away from the storm) will be used to monitor the diurnal pulse propagation throughout the local morning hours and signs of arc cloud formation.

As arc clouds propagate away from the tropical disturbance, they visibly emerge from underneath the central dense overcast that can obscure them from visible an infrared satellite view. Therefore, when arc clouds are identified using satellites, they are often in the middle to later stages of their lifecycles. Hence, the mechanism of enhanced low-level outflow is likely occurring at the time of satellite identification, while the mechanism of cooling/drying of the boundary layer has already occurred (though the effects may still be observable by aircraft flight-level, GPS dropsonde, and satellite data). This necessitates that the arc clouds be identified and sampled as early in their lifecycle as possible using available aircraft observations (e.g. flight-level, GPS dropsonde and P-3 LF radar, and P-3/G-IV Doppler radar data) and satellite imagery (e.g. TC diurnal cycle infrared, visible, infrared, and microwave).

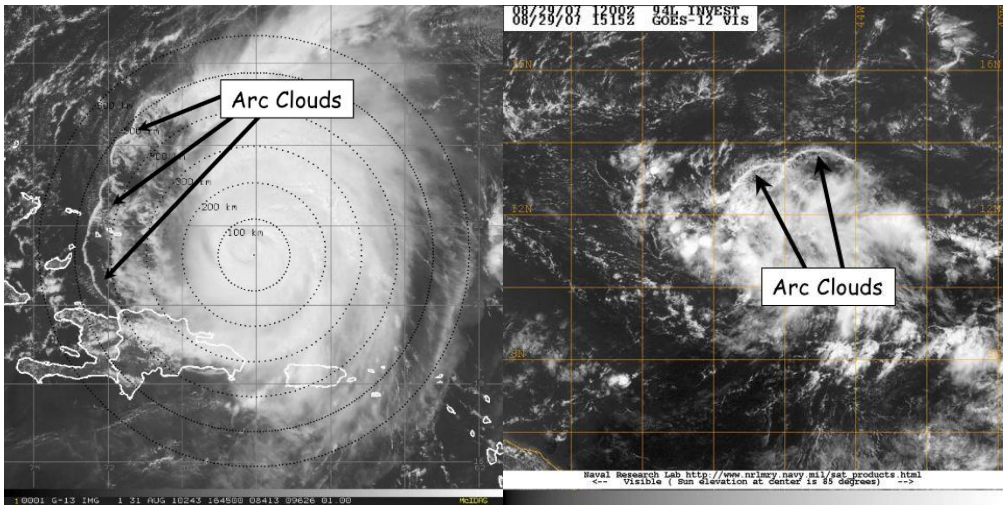

Figure MA-2. *GOES visible satellite imagery showing arc clouds racing away from the convective cores of (left) 2003 Hurricane Isabel and (right) 2007 Pre-Tropical Depression Felix.*

MATURE STAGE EXPERIMENT
Science Description

Hypotheses (Arc Cloud): Arc clouds form along the leading edge of TC diurnal pulses, are particularly favored to occur at R~105–215 n mi (~200–400 km) in areas with mid-level (~600–800-hPa) dry air (≤ 45 mm total precipitable water [TPW]), and can act to temporarily stabilize the TC environment.

Aircraft Pattern/Module Descriptions:

P-3 Module #1: Environment Interaction (Arc Cloud)
G-IV Module #1: Environment Interaction (Arc Cloud)

When arc clouds emanating from the periphery of the TC convective core are identified using satellite imagery and/or P-3 LF radar, perform this break-away pattern by transecting orthogonally across to these outwardly propagating features.

Analysis Strategy (Arc Cloud): This experiment seeks to collect observations across arc cloud features in the periphery of mature TCs using aircraft flight-level, GPS dropsonde, and TDR data to improve our understanding of the physical processes responsible for their formation and evolution, as well as how these features may affect TC structure and intensity in the short-term. Flight-level and GPS dropsonde data will be used to calculate changes in static stability and possible impacts on surface fluxes both ahead of and behind the arc cloud (e.g. enhanced stability/reduced surface fluxes behind the arc cloud leading edge). TDR data will be used to define the vertical structure of the kinematics ahead of, across and behind the arc cloud. Finally, kinematics and thermodynamics associated with arc cloud events will be compared to corresponding locations in model analysis fields (e.g. GFS and HWRF).

References (Arc Cloud):

Dunion, J.P., 2011: Rewriting the climatology of the tropical North Atlantic and Caribbean Sea atmosphere. *J. Climate,* **24***,* 893-908.

Knaff, J.A., and J.F. Weaver, 2010: A mesoscale low-level thunderstorm outflow boundary associated with Hurricane Luis. *Mon. Wea. Rev.,* **128***,* 3352-3355.

MATURE STAGE EXPERIMENT
Science Description

SCIENCE OBJECTIVE #3: *Test new (or improved) technologies with the potential to fill gaps, both spatially and temporally, in the existing suite of airborne measurements in mature hurricanes. These measurements include improved three-dimensional representation of the hurricane wind field, more spatially dense thermodynamic sampling of the boundary layer, and more accurate measurements of ocean surface winds*
[New Observing Systems (NOS)]

COYOTE

Motivation (Coyote): Reducing the uncertainty associated with TC intensity forecasts remains a top priority of NWS/NHC. In addition to NOAA's operational requirements (sampling surface wind and thermodynamic structure), developing the capability to regularly fly low altitude unmanned aerial system (UAS) into TCs helps to advance NOAA research by allowing scientists to sample and analyze a region of the storm that would otherwise be impossible to observe in detail (due to the severe safety risks associated with manned reconnaissance). It is believed that such improvements in basic understanding are likely to improve future numerical forecasts of TC intensity change. Over time, projects such as this, which explore the utilization of unconventional and innovative technologies in order to more effectively sample critical regions of the storm environment should help reduce this inherent uncertainty.

Background (Coyote): Coyote is an electric-powered unmanned aircraft with 1-hour endurance and is built by the Raytheon Company (formerly Sensintel Corporation and British Aerospace Engineering [BAE]). In many ways, this UAS platform can be considered a 'smart GPS dropsonde system' since it is deployed in similar fashion and currently utilizes a comparable meteorological payload similar to systems currently used by NOAA on the GIV and P-3 dropsonde systems. The Coyote can be launched from a P-3 sonobuoy tube in flight, and collects in-situ measurements of temperature, relative humidity, pressure, and remotely senses sea surface temperature. The three-dimensional wind field can be determined using the aircraft's GPS changes in position. Unlike the GPS dropsonde, however, the Coyote UAS can be directed from the NOAA P-3 to specific areas within the storm circulation (both in the horizontal and in the vertical). Furthermore, Coyote observations are continuous in nature and give scientists an extended look into important small-scale thermodynamic and kinematic physical processes that regularly occur within the near-surface boundary layer environment. The Coyote, when operated within a hurricane environment, provides a unique observation platform from which the low-level atmospheric boundary layer environment can be diagnosed in great detail.

Hypotheses (Coyote): 360-degree depictions of hurricane boundary layer RMW and Vmax are possible by conducting UAS eyewall orbit missions that continually synchronize the prevailing wind direction with UAS heading.

Aircraft Pattern/Module Descriptions:

P-3 Module #1: NOS (Coyote, Eyewall A)
P-3 Module #2: NOS (Coyote Eyewall B)

For Coyote Eyewall module: "Sun Pattern" or "Pizza Slice" Pattern

P-3 Module #3: NOS (Coyote, Inflow)

For Coyote Inflow module: modified Lawnmower pattern

Analysis Strategy (Coyote): The analysis of these data includes two components: understanding hurricane boundary layer structure and potential improvements to hurricane prediction that UAS observations provide. Three Coyote working groups analyze existing Coyote data and are focused on three main areas: boundary layer thermodynamics, boundary layer turbulence, and observing system experiments. The understanding of boundary layer physics (both kinematic and thermodynamic processes) uses observations to understand the smaller scale features captured using Coyote data and evaluates the representation of the boundary layer in various model physics schemes using data assimilation (DA) and other statistical techniques. Multiple models and DA schemes will continue to be used for these analyses. Observing system experiments (OSEs) and observing system simulation experiments (OSSEs) can quantify the impact of Coyote observations and allow help optimize Coyote resources by comparing observing strategies generated from a Nature Run. Multiple Nature Runs exist and will be used for these OSSEs in conjunction with appropriate forecast models and DA schemes. These include but are not limited to HWRF, WRF-ARW, and GFS models; and ensemble-based DA systems such as HRD's in-house Hurricane Ensemble Data Assimilation System (HEDAS), as well as 3- and 4-dimensional hybrid DA schemes typically used in operations.

References (Coyote): N/A

NESDIS OCEAN WINDS

Motivation (Ocean Winds): This effort aims to improve our understanding of microwave scatterometer retrievals of the ocean surface wind field and to evaluate new remote sensing techniques/technologies. The NOAA/NESDIS/Center for Satellite Applications and Research in conjunction with the University of Massachusetts (UMASS) Microwave Remote Sensing Laboratory, the NOAA/AOML/Hurricane Research Division, and the NOAA/OMAO/Aircraft Operations Center have been conducting flight experiments during hurricane season for the past several years. The Ocean Winds experiment is part of an ongoing field program whose goal is to further our understanding of microwave scatterometer and radiometer retrievals of the ocean surface winds in high wind speed conditions and in the presence of rain for all wind speeds. This

knowledge is used to help improve and interpret operational wind retrievals from current and future satellite-based sensors. The hurricane environment provides the adverse atmospheric and ocean surface conditions required.

The Imaging Wind and Rain Airborne Profiler (IWRAP), which is also known as the Advanced Wind and Rain Airborne Profiler (AWRAP), was designed and built by the University of Massachusetts and is the critical sensor for these experiments. IWRAP/AWRAP consists of two dual-polarized, dual-incidence angle radar profilers operating at Ku-band and at C-band, which measure profiles of volume reflectivity and Doppler velocity of precipitation in addition to the ocean surface backscatter. Currently the C-band portion of IWRAP has been installed with the prototype antenna for EUMETSAT's ASCAT follow-on satellite sensor that will be launched on EPS-SG. This antenna, on loan from ESA, is a dual-polarized slotted waveguide antenna which allows us to measure the cross-polarized response of the ocean surface, which is a new capability being implemented for the ASCAT follow-on sensor. The Stepped-Frequency Microwave Radiometer (SFMR) and GPS dropsonde system are also essential instrumentation on the NOAA-P3 aircraft for this effort. The NASA GORE (GNSS reflection) system has also been utilized to collect measurements to support the NASA CYGNSS mission, but future plans call for utilizing an improved GNSS-R receiver being developed by the CYGNSS project at the University of Michigan. A Ka-band radar system is being currently developed to enable finer resolution measurements at the air-sea boundary to help decouple what is happening at the interface in the storm environment.

Background (Ocean Winds): The Ocean Winds P-3 flight experiment program has several objectives:

- Calibration and validation of satellite-based ocean surface vector wind (OSVW) sensors such as ASCAT, ScatSat, OceanSat-3 and the new CYGNSS mission that uses GNSS-R techniques to infer the ocean wind speed.
- Product improvement and development for current and planned satellite-based sensors (ASCAT, ScatSat, OceanSat-3, CYGNSS and SCA)
- Testing of new remote sensing technologies for possible future satellite missions (risk reduction) such as the dual-frequency scatterometer concept. A key objective for this year will be the collection of cross-polarized data at C-band to support ESA and EUMETSAT studies for the ASCAT follow-on (SCA), which will be part of their EPS-SG satellite series.
- Advancing our understanding of broader scientific questions such as:
    - Rain processes in tropical cyclones and severe ocean storms: the coincident dual-polarized, dual-frequency, dual-incidence angle measurements would enable us to improve our understanding of precipitation processes in these moderate to extreme rainfall rate events.
    - Atmospheric boundary layer (ABL) wind fields: the conical scanning sampling geometry and the Doppler capabilities of this system provide a unique source of measurements from which the ABL winds can be derived. The advanced digital receivers and data acquisition system recently

implemented will enable to potentially retrieve the wind and reflectivity profiles essentially to the surface.

- Analysis of boundary layer rolls: linearly organized coherent structures are prevalent in tropical cyclone boundary layers, consisting of an overturning "roll" circulation in the plane roughly perpendicular to the mean flow direction. IWRAP has been shown to resolve the kilometer-scale roll features, and the vast quantity of data this instrument has already collected offers a unique opportunity to study them.
- Drag coefficient, Cd: extending the range of wind speeds for which the drag coefficient is known is of paramount importance to further our understanding of the coupling between the wind and surface waves under strong wind forcing, and has many important implications for hurricane and climate modeling. The advanced digital receivers and data acquisition capability allows us to retrieve wind and reflectivity profiles closer to the ocean surface, which can also be exploited to derive drag coefficients by extrapolating the derived wind profiles down to 0 m altitude.

Hypotheses (Ocean Winds): We don't fully understand what is happening at the air-sea interface in extreme storm conditions but it should be possible to characterize this with the proper instrumentation and data collection methodologies.

Aircraft Pattern/Module Descriptions:

P-3 Pattern #1: NOS (Ocean Winds)

The sensitivity of the IWRAP/AWRAP system defines the preferred flight altitude to be below 10,000 ft to enable the system to still measure the ocean surface in the presence of rain conditions typical of tropical systems. With the Air Force Reserve typically flying at 10,000 ft pressure altitude, we have typically ended up with an operating altitude of 7,000 ft radar. Operating at a constant radar altitude is desired to minimize changes in range and thus measurement footprint on the ground. Higher altitudes would limit the ability of IWRAP/AWRAP to consistently see the surface during intense precipitation, but these altitudes would still provide useful data, such as measurements through the melting layer, to study some of the broader scientific questions.

Maneuvers:

Straight and level flight with a nominal pitch offset unique to each P-3 is desired during most flight legs. Constant bank circles of 10–30 degrees have been recently implemented, as a method to obtain measurements at incidence angles greater than the current antenna was configured for. These would be inserted along flight legs where the desired environmental conditions were present. Generally it would be a region of no rain and where we might expect the winds to be consistent over a range of about 6–10 miles, about the diameter of a circle.

This would not be something we would want to do in a strong wind gradient region where the conditions would change significantly while circling.

Patterns:

Typically an ideal Ocean Winds flight pattern would include a survey pattern (Figure-4 or Butterfly) that extended about 50 n mi from the storm center. The actual distance would be dictated by the storm size and safety of flight considerations. Dependent upon what was observed during the survey pattern radial legs in and out of different sectors of the storm focusing on different wind and/or rain conditions.

Storm Types:

The ideal Ocean Winds storm would typically be in a hurricane (category 1 and above) where a large range of wind speeds and rain rates would be found. However, data collected within TDs and TSs would still provide useful observations of rain impacts on the surface observation.

Analysis Strategy (Ocean Winds): TBD

References (Ocean Winds): N/A